IEEE Access
Multidisciplinary | Rapid Review | Open Access Journal

Received December 12, 2018, accepted February 6, 2019, date of publication February 20, 2019, date of current version March 12, 2019.

Digital Object Identifier 10.1109/ACCESS.2019.2900279

Analysis of the Code Phase Migration and Doppler Frequency Migration Effects in the Coherent Integration of Direct-Sequence Spread-Spectrum Signals

YUYAO SHEN AND YING XU
Academy of Opto-Electronics, Chinese Academy of Sciences, Beijing 100094, China

Corresponding author: Ying Xu (nadinexy@aoe.ac.cn)

This work was supported in part by the China Postdoctoral Science Foundation under Grant 2018M631576, in part by the National Postdoctoral Program for Innovative Talents under Grant BX201700246, and in part by the Youth Innovation Promotion Association of CAS under Grant Y50301A1BY.

ABSTRACT Coherent integration of direct-sequence spread-spectrum (DSSS) signals is a commonly used technique to improve receiver performance. However, this approach is susceptible to the code phase migration (CPM) and Doppler frequency migration (DFM) effects resulting from the relative motion between transmitter and receiver. In this paper, the CPM and DFM effects are explored and characterized. To evaluate the CPM effect, a simple analytic expression for the coherent integration results under motions of arbitrary orders is developed. In addition, the theoretically derived integration loss and time synchronization error caused by CPM are quantitatively examined. The DFM effect is evaluated under the motions of arbitrary orders by Fresnel integration and numerical fitting. The obtained closed-form expressions are verified by simulation and are shown to be useful for the performance analysis and the DSSS receiver design. The theoretical and the numerical results show that when the amount of CPM is larger than about one code chip duration, the signal-to-noise ratio gain obtained by coherent integration no longer increases because of the integration loss caused by CPM. In addition, the integration loss (in decibel units) caused by DFM is approximately inversely proportional to the square of the time–bandwidth product when the time–bandwidth product is small, and it is inversely proportional to the logarithm of the time–bandwidth product when this product is large.

INDEX TERMS Arbitrary motion order, code phase migration, coherent integration, Doppler frequency migration, direct-sequence spread-spectrum (DSSS), motion effect.

I. INTRODUCTION

Direct-sequence spread-spectrum (DSSS) signals are widely used in communication systems, in the global navigation satellite system, and in telemetry, tracking and command systems, to name just a few examples. Coherent integration of these signals is commonly used to improve receiver performance [1]. However, the relative motions between transceivers may generate Doppler frequency migration (DFM) and code phase migration (CPM) [2] during integration, leading to integration loss and synchronization errors. It is therefore crucial to investigate these effects quantitatively and mitigate them. Some resolutions, such as the ACCF [3] and GRFT [4], have been proposed to solve the CPM and DFM. In this study, we attempt to analyze their influence.

The influence of range migration (RM) and DFM has recently been studied in the context of chirp signals in radar applications, and some corresponding solutions have been proposed [5]–[7]; the related issues in DSSS applications have received less attention.

The RM/CPM effect—the effect of motion on the modulated baseband waveform—results in an envelope migration of the integration result in the time-delay dimension [8].

The associate editor coordinating the review of this manuscript and approving it for publication was Zilong Liu.

Therefore, the conclusions concerning the RM problem obtained for chirp signals are not directly applicable to the CPM problem within the context of DSSS signals. Moreover, the previous studies on RM in chirp signals [9] considered only velocity and acceleration, and closed-form expressions were not provided. Based on the correlation properties of the pseudo-noise (PN) codes used in DSSS signals, an analytic expression for the CPM effect as a function of velocity was obtained in [10].

The DFM effect—which can be regarded as the effect of motion on the carrier—has a similar expression in both radar (with chirp signals) and DSSS communication applications, the difference being the factor of two resulting from the direct path versus round-trip delay contexts. Therefore, the DFM results obtained for chirp signals can be applied to DSSS signals with only a coefficient amendment. In [9], the results of integration with DFM were modeled as polynomial phase signals [11]–[14]; the optimal and threshold integration times were obtained by simulation and numerical fitting, assuming that the motion components of orders higher than two (acceleration) [15] or three (jerk) [16] could be omitted.

All the literature works mentioned above explore the RM/CPM and DFM effects under lower order motions. The second-order motion (acceleration) and third-order (jerk) motions have not been examined adequately. However, it is necessary to expand this result to higher-order motions in order to account for increased dynamics, longer integration times, and super-resolution time-delay estimation demands, and also, to achieve a comparatively complete theory.

This paper presents a closed-form analytic expression for the integration of signals affected by CPM under arbitrary-order motions. The integration loss, time synchronization error, optimal integration time—from a signal-to-noise-ratio (SNR) point of view—and threshold integration time—from a synchronization error point of view—are also examined. The DFM effects are analyzed using the principle of stationary phase and numerical analysis. The main contribution of this paper is the extension to higher-order motion situations in previously existing integration performance analyses for the specific cases of second- and third-order motion. In addition, this study derives generalized equations applicable to motions of arbitrary order. The derived expressions are verified through simulation, and can be used to not only evaluate integration performance but also guide motion order configuration of the received signal and optimize receiver design.

The remainder of this paper is organized as follows. The signal model is introduced in Section II, and the CPM and DFM effects are analyzed in Sections III and IV, respectively. Section V presents some numerical results to validate the analytical work. Finally, conclusions are drawn in Section VI.

II. SIGNAL MODEL

To speed up the acquisition of DSSS signals with large uncertainty in the Doppler dimension, a partial matched filter-fast Fourier transform (FFT) architecture is generally used, in which the received digital baseband DSSS signal must be segmented. Let us assume that the inter-segment and intra-segment indices are denoted by $k(k = 0, 1, 2, \ldots, K-1)$ and n $(n = 0, 1, \ldots, N-1)$, respectively; the intra-segment sampling times are therefore $T_n = nT_s$, and the segment starting time instants are $T_k = kNT_s$, where T_s denotes the sampling interval. The received baseband signal can therefore be expressed as

$$\begin{aligned} &x\left(T_n+T_k\right) \\ &\quad = A\times D\left[T_n+T_k-\tau\left(n,k\right)\right]C\left[T_n+T_k-\tau\left(n,k\right)\right] \\ &\qquad \times\exp\left[-j2\pi f_0\tau\left(n,k\right)\right]+w\left(T_n+T_k\right), \end{aligned} \tag{1}$$

where A and f_0 denote the amplitude and carrier frequency, respectively; $D(t)$, $C(t)$, and $w(t)$ represent the data, PN code, and additive white Gaussian noise component, respectively; $\tau(n,k)$ is the instantaneous transmitting delay. As is customary, the CPM and high-order DFM within the segment duration is omitted, because NT_s is relatively small [3]. Then (1) can be expressed as

$$\begin{aligned} x\left(T_n+T_k\right) &= A\times D\left[T_n+T_k-\tau\left(k\right)\right]C\left[T_n+T_k-\tau\left(k\right)\right] \\ &\quad\times\exp\left[-j2\pi f_0\tau\left(k\right)\right]\exp\left(-j2\pi f_0a_1T_n\right) \\ &\quad+w\left(T_n+T_k\right), \end{aligned} \tag{2}$$

$\tau(k)$ is the degenerated instantaneous transmitting delay that can be expressed as

$$\tau\left(k\right)=\frac{r\left(k\right)}{c}=\tau_0+\sum_{i=1}^{\infty}\frac{a_i}{i!}\left(T_k\right)^i, \tag{3}$$

where $r(k)$ denotes the instantaneous range between transmitter and receiver, which is modeled as a polynomial function in terms of motion parameters [3], c is the velocity of light, τ_0 denotes the initial time delay (corresponding to the initial range), and $\sum_{i=1}^{\infty}a_i\left(T_k\right)^i/i!$ denotes the time delay caused by CPM. Herein, i denotes the motion order, and a_i denotes the corresponding motion parameter normalized by c; in particular, a_1 and a_2 denote the normalized velocity and acceleration, respectively.

Denoting the candidate estimates of the initial time delay by τ, the local replica is then

$$z\left(T_n+T_k\right)=C\left(T_n+T_k-\tau\right). \tag{4}$$

Therefore, the coherent integration results can be derived as

$$\begin{aligned} R\left(\tau,f\right) &= \sum_{k=0}^{K-1}\left[\sum_{n=0}^{N-1}x\left(T_n+T_k\right)z^*\left(T_n+T_k\right)\right]\exp\left(-j2\pi fT_k\right) \\ &= \sum_{k=0}^{K-1}AN\times R_c\left[\tau-\sum_{i=0}^{\infty}\frac{a_i}{i!}\left(T_k\right)^i\right]R_f\left(f\right)+w'\left(\tau,f\right), \end{aligned} \tag{5}$$

where $*$ is the conjugate operator, and w' denotes the integrated noise component. In this paper, only the effect of motion is analyzed; therefore, the data component is always assumed to be 1, i.e., the data sign transition within the integration period are assumed to have been eliminated [17], [18].

R_c and R_f are the normalized correlations of the segmented code and carrier component, respectively, and are defined as

$$R_c\left[\tau-\sum_{i=0}^{\infty}\frac{a_i}{i!}\left(T_k\right)^i\right] = \frac{1}{N}\sum_{n=0}^{N-1}\left\{C\left[T_n+T_k-\tau\left(k\right)\right]C^*\left(T_n+T_k-\tau\right)\right\}, \quad (6)$$

and

$$\begin{aligned} R_f\left(f\right) &= \exp\left[-j2\pi f_0\tau\left(k\right)\right]\exp\left(-j2\pi fT_k\right) \\ &\quad\times\frac{1}{N}\sum_{n=0}^{N-1}\exp\left(-j2\pi f_0a_1T_n\right) \\ &= \exp\left(-j\pi f_0a_1T_N\right)\sin c\left(\pi f_0a_1T_N\right) \\ &\quad\times\exp\left[-j2\pi f_0\tau\left(k\right)\right]\exp\left(-j2\pi fT_k\right), \end{aligned} \quad (7)$$

where $\sin c\left(x\right)=\sin\left(x\right)/x$.

According to the integration results, $R_c\left(\tau\right)$ and $R_f\left(f\right)$ are two separate entities, which allows CPM and DFM to be discussed separately. The integrated motion effect can be analyzed by simply multiplying these values.

Considering only the signal component and the effect of CPM, the coherent integration results can be rewritten as

$$I_c\left(\tau\right)=\frac{1}{K}\sum_{k=0}^{K-1}R_c\left[\tau-\tau_0-\sum_{i=1}^{\infty}\frac{a_i}{i!}\left(T_k\right)^i\right], \quad (8)$$

where $R_c\left(\tau\right)$ is $1-|\tau|/T_c$ if $|\tau|\le T_c$, and 0 otherwise, T_c being the code chip duration. Therefore, if $a_i\equiv 0$ for $i=1,2,\ldots,\infty$, R_c can reach its maximum value at the same τ for all k. In this case, the maximum value of $I_c\left(\tau\right)$ is 1; otherwise, $I_c\left(\tau\right)$ will be less than 1, and an integration loss will occur because of CPM. Furthermore, when $\tau-\tau_0=\sum_{i=1}^{\infty}a_i\left(T_k\right)^i/i!$, R_c reaches its maximum segmental value, and the segmental estimation error of the initial time delay may lead to an overall estimation error that exceeds the time-delay resolution (i.e., half the sampling interval). Therefore, a time synchronization error will occur because of CPM.

In (7), $\exp\left(-j\pi f_0a_1T_N\right)$ is a phase item which will not bring about any integration loss; $\sin c\left(\pi f_0a_1T_N\right)$ represents the integration loss caused by the first-order DFM within the segment duration, which has been well examined by many literatures. Therefore, only the effect of the remaining part, i.e., $\exp\left[-j2\pi f_0\tau\left(k\right)\right]\exp\left(-j2\pi fT_k\right)$, will be analyzed in this paper. Considering only the signal component, the coherent integration results corresponding to the remaining effect of DFM can be rewritten as

$$I_f\left(f\right)=\frac{1}{K}\sum_{k=0}^{K-1}\left\{\exp\left[-j2\pi\sum_{i=1}^{\infty}\frac{a_i}{i!}f_0\left(T_k\right)^i\right]\exp\left(-j2\pi fT_k\right)\right\}. \quad (9)$$

Therefore, if $a_i\equiv 0$ for $i=2,\ldots,\infty$, R_f can reach its maximum value at the same f for all k. In this case, the maximum value of $I_f\left(f\right)$ is 1; otherwise, $I_f\left(f\right)$ will be less than 1, and an integration loss will occur because of DFM. Furthermore, when $f+a_1f_0=-\sum_{i=2}^{\infty}a_if_0\left(T_k\right)^{i-1}/i!$, R_f reaches its maximum segmental value, and the segmental estimation error of the initial Doppler frequency may lead to an overall estimation error that exceeds the Doppler frequency resolution (i.e., half the value of $1/T_K$). Therefore, a frequency synchronization error will occur because of DFM.

Based on the signal model presented above, this paper divides the motion effect issue into two aspects—the CPM effects and the DFM effects—and discusses them separately in the following two sections, as shown in Fig. 1.

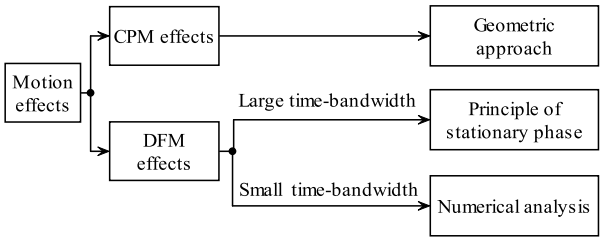

FIGURE 1. Diagram of the proposed solutions to the analysis of motion effects consisting of CPM and DFM effects.

It is worth noting that the CPM and DFM effects are determined by all the motion parameters, whose directions may be diverse and cannot be pre-determined in practice; this makes it difficult to obtain a closed-form solution to the integration according to the *Descartes' rule of signs*. However, as a compromise solution, the CPM and DFM effects can be decomposed according to the individual motion orders, and then analyzed separately for each of those orders. Doing this is valuable because the single-order motion analyses provide bounds for the combined-order motion cases. In addition, the effect of the combined-order motion sometimes approximates the sum of the effects of each motion order taken separately. Furthermore, this approach provides guidance for motion order configuration when modeling a specific received signal, as well as for the selection and evaluation of the dynamic focus algorithm (see Section V.D). Analyzing each order of motion individually is similar to what is done in many motion estimation and compensation methods [3], [4], in which the motions are treated successively. Therefore, in the following two sections, the integration results are calculated for each motion parameter separately.

III. CODE PHASE MIGRATION EFFECTS

In this section, the code phase migration effects are theoretically derived.

Assuming that all motion parameters other than a_i are compensated, (8) can be simplified to

$$S\left(\tau\right)=\frac{1}{K}\sum_{k=0}^{K-1}R_c\left[\delta\tau-\frac{a_i}{i!}\left(T_k\right)^i\right], \quad (10)$$

where $\delta\tau$ stands for $\tau-\tau_0-\sum_{l=1,l\ne i}^{\infty}\delta a_l\left(T_k\right)^l/l!$. Herein δa_l is the residual motion parameter, which—for simplicity—is assumed to be zero in the following derivations.

A. CLOSED-FORM EXPRESSION FOR THE INTEGRATION RESULTS

To obtain a closed-form expression of (10), a geometric approach is proposed. The code correlation function is an isosceles triangle within a limited delay range; all the K code segment correlations can be aligned to form a prism bended along the k-axis because of the time-varying CPM [see Fig. 2(a)]. The integration result in (10) can then be identified with the area of the shadowed cross section represented in Fig. 2(a), which is a slice corresponding to a given $\delta\tau$.

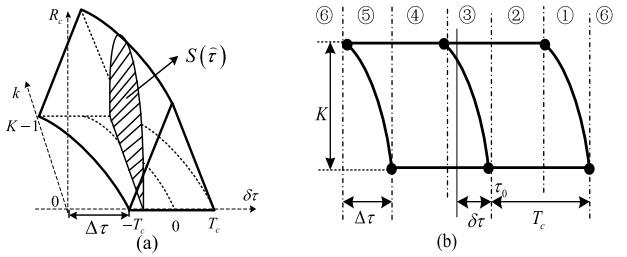

FIGURE 2. Geometric representation of the integration affected by CPM. (a) 3D image. (b) Planform of the correlation prism.

The maximum delay increment caused by CPM (labeled as $\Delta\tau$ in Fig. 2) is $a_i (T_K)^i/i!$. According to the value of $\Delta\tau$, the computation of (10) may be divided into three cases.

Case 1 ($0 \le \Delta\tau < T_c$):

The integration is a piecewise function of $\delta\tau$, which can be divided into six sections, according to the intersection points marked by dots in Fig. 2(b)—the planform of Fig. 2(a). Five of these sections are illustrated in Fig. 3; the remaining section corresponds to the slices located outside the bended prism, i.e., $\{\delta\tau \,|\, \delta\tau > \Delta\tau + T_c \text{ or } \delta\tau < -T_c\}$.

The upper and lower integration limits in (10) can be obtained according to the range of $\delta\tau$. The corresponding integration results can be written as (see Appendix A for the mathematical derivation of these results)

$$S(\delta\tau) = \begin{cases} \dfrac{i(T_c+\delta\tau)^{1+1/i}}{(i+1)T_c\Delta\tau^{1/i}}, & -T_c \le \delta\tau < \Delta\tau - T_c \\ 1 - \dfrac{\Delta\tau - (i+1)\delta\tau}{(i+1)T_c}, & \Delta\tau - T_c \le \delta\tau < 0 \\ 1 + \dfrac{\delta\tau}{T_c} - \dfrac{2i(\delta\tau)^{1+1/i} + \Delta\tau^{1+1/i}}{(i+1)T_c\Delta\tau^{1/i}}, & 0 \le \delta\tau < \Delta\tau \\ 1 - \dfrac{\delta\tau}{T_c} + \dfrac{\Delta\tau}{(i+1)T_c}, & \Delta\tau \le \delta\tau < T_c \\ 1 - \dfrac{\delta\tau}{T_c} + \dfrac{i(\delta\tau - T_c)^{1+1/i} + \Delta\tau^{1+1/i}}{(i+1)\Delta\tau^{1/i}}, & T_c \le \delta\tau \le \Delta\tau + T_c \\ 0, & \text{others.} \end{cases} \tag{11}$$

The integration results can be similarly obtained for the other ranges of $\Delta\tau$, i.e., $T_c \le \Delta\tau \le 2T_c$ and $\Delta\tau \ge 2T_c$, as presented below; the only difference lies in the variation of the relative position of the intersection points, as shown in Figs. 4(a) and 4(b).

Case 2 ($T_c \le \Delta\tau < 2T_c$):

$$S(\delta\tau) = \begin{cases} \dfrac{i(T_c+\delta\tau)^{1+1/i}}{(i+1)T_c\Delta\tau^{1/i}}, & -T_c \le \delta\tau < 0 \\ \dfrac{i(T_c+\delta\tau)^{1+1/i} - 2i(\delta\tau)^{1+1/i}}{(i+1)T_c\Delta\tau^{1/i}}, & 0 \le \delta\tau < \Delta\tau - T_c \\ 1 + \dfrac{\delta\tau}{T_c} - \dfrac{2i(\delta\tau)^{1+1/i} + \Delta\tau^{1+1/i}}{(i+1)T_c\Delta\tau^{1/i}}, & \Delta\tau - T_c \le \delta\tau < T_c \\ 1 + \dfrac{\delta\tau}{T_c} - \dfrac{2i(\delta\tau)^{1+1/i} + \Delta\tau^{1+1/i} - i(\delta\tau - T_c)^{1+1/i}}{(i+1)T_c\Delta\tau^{1/i}}, & T_c \le \delta\tau < \Delta\tau \\ 1 - \dfrac{\delta\tau}{T_c} + \dfrac{\Delta\tau^{1+1/i} + i(\delta\tau - T_c)^{1+1/i}}{(i+1)T_c\Delta\tau^{1/i}}, & \Delta\tau \le \delta\tau \le \Delta\tau + T_c \\ 0, & \text{others.} \end{cases} \tag{12}$$

Case 3 ($\Delta\tau \ge 2T_c$):

$$S(\delta\tau) = \begin{cases} \dfrac{i(T_c+\delta\tau)^{1+1/i}}{(i+1)T_c\Delta\tau^{1/i}}, & -T_c \le \delta\tau < 0 \\ \dfrac{i(T_c+\delta\tau)^{1+1/i} - 2i(\delta\tau)^{1+1/i}}{(i+1)T_c\Delta\tau^{1/i}}, & 0 \le \delta\tau < T_c \\ \dfrac{i(T_c+\delta\tau)^{1+1/i} + i(\delta\tau - T_c)^{1+1/i} - 2i(\delta\tau)^{1+1/i}}{(i+1)T_c\Delta\tau^{1/i}}, & T_c \le \delta\tau < \Delta\tau - T_c \\ 1 + \dfrac{\delta\tau}{T_c} - \dfrac{2i(\delta\tau)^{1+1/i} + \Delta\tau^{1+1/i} - i(\delta\tau - T_c)^{1+1/i}}{(i+1)T_c\Delta\tau^{1/i}}, & \Delta\tau - T_c \le \delta\tau < \Delta\tau \\ 1 - \dfrac{\delta\tau}{T_c} + \dfrac{\Delta\tau^{1+1/i} + i(\delta\tau - T_c)^{1+1/i}}{(i+1)T_c\Delta\tau^{1/i}}, & \Delta\tau \le \delta\tau \le \Delta\tau + T_c \\ 0, & \text{others.} \end{cases} \tag{13}$$

Based on these results, the CPM effects—such as integration loss and synchronization error—are examined next.

B. INTEGRATION LOSS

The integration loss η (the ratio of the integrated signal powers with and without CPM influence) is obtained by searching for the maximum value of $|S(\delta\tau)|^2$, i.e.,

$$\eta = \max_{\delta\tau}\left\{|S(\delta\tau)|^2\right\} = \begin{cases} \left(1 - \dfrac{1-2^{-i}}{i+1}\dfrac{\Delta\tau}{T_c}\right)^2, & 0 \le \Delta\tau < \dfrac{T_c}{1-2^{-i}} \\ \left(\dfrac{i}{i+1}\left[\dfrac{T_c}{(1-2^{-i})\Delta\tau}\right]^{1/i}\right)^2, & \Delta\tau \ge \dfrac{T_c}{1-2^{-i}}. \end{cases} \tag{14}$$

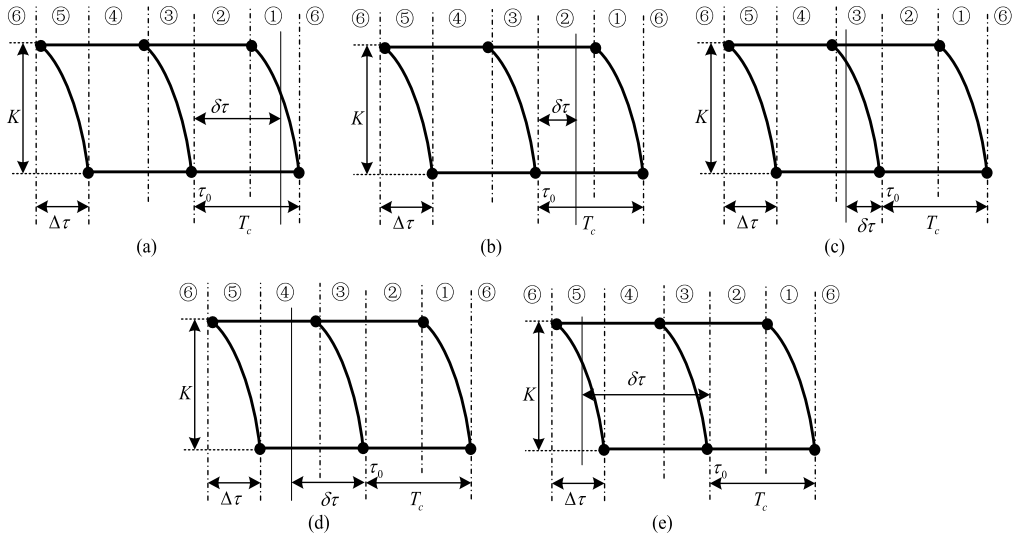

FIGURE 3. Planform of the correlation prism when $0 \le \Delta\tau < T_c$ (which provides a comprehensive approach to obtain the upper-lower limit and integrand function of the integration). (a) $-T_c \le \delta\tau < \Delta\tau - T_c$. (b) $\Delta\tau - T_c \le \delta\tau < 0$. (c) $0 \le \delta\tau < \Delta\tau$. (d) $\Delta\tau \le \delta\tau < T_c$. (e) $T_c \le \delta\tau \le \Delta\tau + T_c$.

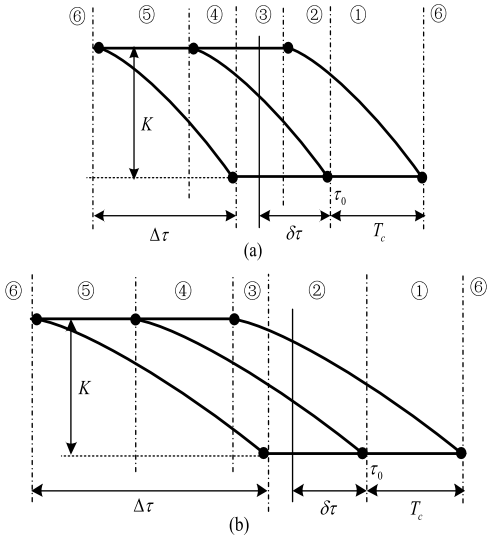

FIGURE 4. Planform of the correlation prism (which provides a comprehensive approach to obtain the upper-lower limit and integrand function of the integration). (a) $T_c \le \Delta\tau \le 2T_c$. (b) $\Delta\tau \ge 2T_c$.

The solution to this maximization problem was obtained by setting the derivatives of $S(\delta\tau)$ to zero; additionally, when $b \le a$ and $0 < c < 1$, $(a+b)^c + (a-b)^c \le 2a^c$ was used. The detailed derivations are presented in Appendix B.

C. SNR GAIN AND OPTIMAL INTEGRATION TIME

The SNR gain G is the product of the integration loss and the ideal SNR gain G_{ideal}, which can be denoted as

$$G_{ideal} = B_{in} T_K, \tag{15}$$

B_{in} being the input signal's bandwidth and T_K the integration time. Therefore,

$$G = \eta G_{ideal} = \begin{cases} B_{in} T_K \left(1 - \dfrac{1-2^{-i}}{i+1} \dfrac{a_i T_K^i}{i! T_c}\right)^2, & 0 \le \Delta\tau < \dfrac{T_c}{1-2^{-i}} \\ \dfrac{B_{in}}{T_K} \left(\dfrac{i}{i+1} \left[\dfrac{i! T_c}{\left(1-2^{-i}\right) a_i}\right]^{1/i}\right)^2, & \Delta\tau \ge \dfrac{T_c}{1-2^{-i}}. \end{cases} \tag{16}$$

Herein, $\Delta\tau = a_i (T_K)^i / i!$ is used in the derivations.

The maximum SNR gain and the corresponding optimal integration time can be found to be

$$G_{opt} = B_{in} \left(\frac{2i}{1+2i}\right)^2 \left[\frac{(i+1)\, i! T_c}{\left(1-2^{-i}\right)(1+2i)\, a_i}\right]^{1/i}, \tag{17}$$

$$T_{opt} = \left[\frac{(i+1)\, i! T_c}{\left(1-2^{-i}\right)(1+2i)\, a_i}\right]^{1/i}. \tag{18}$$

The value of T_{opt} places a restriction on the maximum integration time that can be used in the presence of CPM.

D. SYNCHRONIZATION ERROR AND THRESHOLD INTEGRATION TIME

As mentioned above, CPM leads to time synchronization errors (denoted by ε_τ). This error can be obtained as the

argument that maximizes $S(\delta\tau)$, i.e.,

$$\varepsilon_\tau = \arg\max_{\delta\tau}\left\{|S(\delta\tau)|^2\right\} = \begin{cases} \dfrac{\Delta\tau}{2^i}, & 0 \le \Delta\tau \le \dfrac{T_c}{1-2^{-i}} \\ \dfrac{T_c}{2^i-1}, & \Delta\tau \ge \dfrac{T_c}{1-2^{-i}} \text{ and } i>1 \\ [T_c, \Delta\tau - T_c], & \Delta\tau \ge 2T_c \text{ and } i=1. \end{cases} \quad (19)$$

This shows that when $\Delta\tau \le T_c/(1-2^{-i})$, ε_τ increases linearly with $\Delta\tau$, and stabilizes for $\Delta\tau \ge T_c/(1-2^{-i})$ if $i>1$; when $\Delta\tau \ge 2T_c$ and $i=1$, ε_τ is randomly distributed within $[T_c, \Delta\tau - T_c]$. For fixed a_i, $\Delta\tau$ is a monotonic function of the integration time; therefore, the threshold integration time, defined as the integration time corresponding to $\Delta\tau = T_c/(1-2^{-i})$, is given by

$$T_{th} = \left(\frac{i!}{1-2^{-i}}\frac{T_c}{a_i}\right)^{1/i}. \quad (20)$$

The sign of $\Delta\tau$ determines only the direction of the band of the prism mentioned above; therefore, when $\Delta\tau$ is negative, $\eta(\Delta\tau) = \eta(-\Delta\tau)$, $G(\Delta\tau) = G(-\Delta\tau)$, and $\varepsilon_\tau(\Delta\tau) = -\varepsilon_\tau(-\Delta\tau)$.

IV. DOPPLER FREQUENCY MIGRATION EFFECTS

In this section, the Doppler frequency migration effects are studied using a Fresnel-integral-based approach in the large time-bandwidth product case, and numerical analysis in the small time-bandwidth product case.

Assuming that all motion parameters other than a_i are compensated, (9) can be simplified to

$$S_f(f) = \frac{1}{K}\sum_{k=0}^{K-1}\left\{\exp\left[-j2\pi\frac{a_i}{i!}f_0(T_k)^i\right]\exp(-j2\pi f T_k)\right\}. \quad (21)$$

Given that the integration time is T_K, the signal bandwidth is

$$B = \frac{a_i}{(i-1)!}f_0(T_K)^{i-1}. \quad (22)$$

When the signal's time-bandwidth product is large enough, (21) can be regarded as a Fresnel integral [19], which can be solved using the principle of stationary phase [20]; in all other cases, it must be numerically solved [21].

A. LARGE TIME-BANDWIDTH PRODUCT CONDITIONS

According to the principle of stationary phase, when the signal time-bandwidth product is large enough ($BT_K \gg 1$) we can obtain the stationary point T_k^* as follows

$$T_k^* = \left[-\frac{(i-1)!}{a_i}\frac{f}{f_0}\right]^{1/(i-1)}\mathrm{U}\left(-\frac{f}{a_i}\right), \quad (23)$$

where $\mathrm{U}(\cdot)$ is the unit step function, i.e., $\mathrm{U}(x)=1$ if $x\ge 0$ and 0 otherwise. Herein, function $\mathrm{U}(\cdot)$ ensures that T_k^* is the only solution for the physical significance of the equation in which the phase of (21) equals zero.

In these conditions, (21) can be rewritten as

$$\begin{aligned} S_f(f) &= \mathrm{U}\left(-\frac{f}{a_i}\right)\frac{1}{T_K}\left|(i-1)f\left[-\frac{(i-1)!}{a_i}\frac{f}{f_0}\right]^{-1/(i-1)}\right|^{-1/2} \\ &\quad\times \mathrm{rect}\left(\frac{1}{T_K}\left[-\frac{(i-1)!}{a_i}\frac{f}{f_0}\right]^{1/(i-1)}\right) \\ &\quad\times \exp\left\{-j2\pi\left\{\frac{a_i}{i!}f_0\left[-\frac{(i-1)!}{a_i}\frac{f}{f_0}\right]^{i/(i-1)}\right.\right. \\ &\quad\left.\left.+f\left[-\frac{(i-1)!}{a_i}\frac{f}{f_0}\right]^{1/(i-1)}\right\}\right\} \\ &= \mathrm{U}\left(-\frac{f}{a_i}\right)\left[(i-1)B^{1/(i-1)}T_K|f|^{\frac{i-2}{i-1}}\right]^{-1/2} \\ &\quad\times \mathrm{rect}\left[(|f|/B)^{1/(i-1)}\right] \\ &\quad\times \exp\left\{-j2\pi\left(\frac{i-1}{i}B^{-1/(i-1)}T_K|f|^{\frac{1}{i-1}}f\right)\right\}. \end{aligned} \quad (24)$$

where $\mathrm{rect}(\cdot)$ is a rectangle window function, i.e., $\mathrm{rect}(x)=1$ if $0\le x\le 1$, and $\mathrm{rect}(x)=0$ otherwise.

Maximizing $S_f(f)$ in the f domain, we obtain the DFM integration loss in large time-bandwidth product situations:

$$\begin{aligned} \eta &= \max\left\{\left[(i-1)B^{1/(i-1)}T_K|f|^{\frac{i-2}{i-1}}\right]^{-1/2} \right. \\ &\quad\left.\times\mathrm{rect}\left[(|f|/B)^{1/(i-1)}\right]\right\}^2 \\ &= \max\left\{\frac{\mathrm{rect}\left[(|f|/B)^{1/(i-1)}\right]}{\left[(i-1)B^{1/(i-1)}T_K|f|^{\frac{i-2}{i-1}}\right]}\right\}. \end{aligned} \quad (25)$$

Therefore, when $i=2$, $\eta = 1/(BT_K)$ and the maximum is obtained at $|f|\le B/2$, which indicates that the correlation results in second-order motion situations are multi–peaked in the f domain. When $i>2$, η are impulse functions and the maximum occurs at $f=0$. According to the conducted numerical simulations, η can then be expressed as

$$\eta = (BT_K)^{-2/i}. \quad (26)$$

It is noteworthy to point out that the value of η for $i=2$ is also in good agreement with (26).

The corresponding integration gain can be derived as

$$G_{SNR} = \eta G_{ideal} = \frac{B_{in}T_K}{(BT_K)^{i/2}} = B_{in}\frac{T_K^{(1-i/2)}}{B^{i/2}}, \quad BT_K \gg 1. \quad (27)$$

The larger the time-bandwidth product is, the larger the spectral range diffuses, and the worse the integration performance becomes. Therefore, the optimal integration gain and optimal integration time appear in small time-bandwidth product conditions.

B. SMALL TIME-BANDWIDTH PRODUCT CONDITIONS

When the signal's time-bandwidth product is small, the integration performance must be numerically determined, using computer simulations [9], [21]. The obtained numerical simulation results indicate that the integration performance with DFM is related to the motion order, even if the motion order is higher than three. Therefore, the performance analysis results can be extended from the previously analyzed second [10] and third [16] order cases to higher-order motion situations; a generalized fitting formula to do so is deduced and proved in this section. In contrast with the other order motion conditions, the second-order DFM amount behaves linearly with the integration time. This leads to a multi-peaked integration result in the frequency domain when the integration time is longer than a certain threshold. Therefore, the DFM effect of second-order motion is analyzed separately.

1) SECOND-ORDER MOTION DFM EFFECT

The optimal integration gain and corresponding optimal integration time are [10]

$$G_{SNR,opt} = 1.14\frac{B_{in}}{\sqrt{|a_2|f_0}}, \quad (BT_K)_{opt} = 2.2 \tag{28}$$

$$T_{opt} = \sqrt{\frac{(BT_K)_{opt}}{|a_2|f_0}} = \sqrt{\frac{2.2}{|a_2|f_0}}. \tag{29}$$

When the integration time is longer than a certain threshold value, the integration result has multiple peaks in the frequency domain, which impairs signal detection. This threshold integration time can be expressed as

$$T_{th} = \sqrt{\frac{(BT_K)_{th}}{|a_2|f_0}} = \sqrt{\frac{5.1}{|a_2|f_0}}. \tag{30}$$

2) ARBITRARY-ORDER MOTION DFM EFFECT

In the case of arbitrary-order motion, the obtained numerical simulation results show that the maximum SNR gain has a relationship with the motion order that can be written as

$$G_{SNR,opt}(i) = C_i^G \frac{B_{in}}{(|a_i|f_0)^{1/i}}, \tag{31}$$

where C_i^G is a constant related to the motion order. Combining the second-order motion into this result, the fitting formula for C_i^G is

$$C_i^G = \begin{cases} 1.14, & i = 2 \\ 10^{(-0.04i^2+1.2i-2.13)/10}, & i \geq 3. \end{cases} \tag{32}$$

The corresponding optimal integration time is

$$T_{opt} = C_i^T (|a_i|f_0)^{-1/i}, \tag{33}$$

where constant C_i^T can also be obtained by numerical fitting, resulting in $C_i^T = 10^{(0.55i+0.556)/10}$.

The SNR gain after integration reaches its peak value when the integration time is T_{opt}. Once the integration time reaches T_{opt}, raising the integration time further does not improve the integration gain; however, the computational load still increases. When the integration time is lower than T_{opt}, the integration loss and frequency synchronization error are monotonic functions of the integration time for a given motion parameter, and therefore can be analyzed by numerical fitting.

The integration loss (in decibel units) fitting equation is

$$\eta\ (dB) = -(BT_K)^2\left(i^{-1} - C_i^\eta\right). \tag{34}$$

The fitting values obtained for C_i^η are $C_2^\eta = 0.253$, $C_3^\eta = 0.08$, and $C_i^\eta = 0.064$ for $i > 3$. The results for the different motion parameters are almost coincident, and therefore the integration loss is independent of $a_i f_0$.

The frequency synchronization error fitting equation is

$$\left|\varepsilon_f(i)\right| = C_i^{f1}(|a_i|f_0)^{1/i}(BT_K)^{C_i^{f2}}. \tag{35}$$

The fitting values obtained for C_i^{f1} and C_i^{f2} are $C_i^{f1} = 1.7i^{-2} + 0.2i^{-1} - 0.03$ and $C_i^{f2} = 0.07i + 0.5$, respectively.

V. NUMERICAL RESULTS

In this section, the derived formulas are verified by numerical simulations. The CPM and DFM effect components are evaluated separately.

A. NUMERICAL EVALUATION OF THE CPM EFFECT

Numerical simulations were conducted to evaluate the integration performance in the presence of CPM, and thus verify the expressions derived above. A 1023 bit C/A code with a code rate of 1.023 Mcps was selected as PN code. T_N was 50 μs (which is short enough to ignore the intra-segment CPM effect), T_K ranged from 0.1 s to 3 s, and the corresponding CPM could reach 2.25 chips. The motion parameters were selected to comply with $T_K = 3$ s and $\Delta\tau = 2.25$ chips, i.e., $a_i = i!\Delta\tau/(T_K)^i = i!2.25/\left(1.023 \times 10^6\right)/3^i$; $N = 16384$, which was high enough to allow the evaluation of the synchronization error with motion of orders up to seven. The initial time delay of the simulated received signal was randomly selected, and the subsequent results were obtained with one hundred Monte Carlo runs.

1) INTEGRATION LOSS

Fig. 5 shows the integration loss caused by CPM; in this figure's legend, "Theo" and "Sim" stand for "Theoretical" and "Simulation," respectively. The different orders of motion are represented by dotted lines with different markers. They all coincide with the theoretical results obtained by (14), represented by solid lines. As shown, the integration loss increased with $\Delta\tau$ and decreased with the order of motion.

2) SNR GAIN AND OPTIMAL INTEGRATION TIME

The SNR gain is shown in Fig. 6 as a function of CPM. The ideal and maximum gains are shown with dashed and dashed-dotted lines, ("Ideal" and "Opt" in the legend, respectively). As shown, the actual SNR gain is always below the ideal value, and decreases with decreasing motion order for a

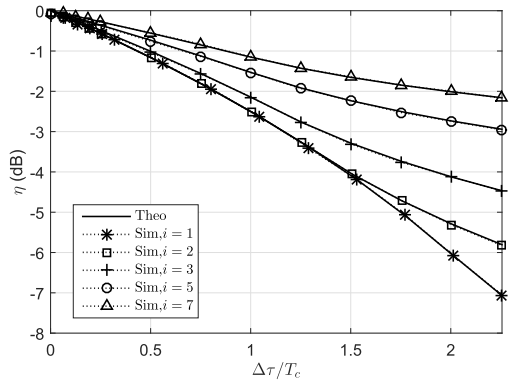

FIGURE 5. Integration loss versus CPM.

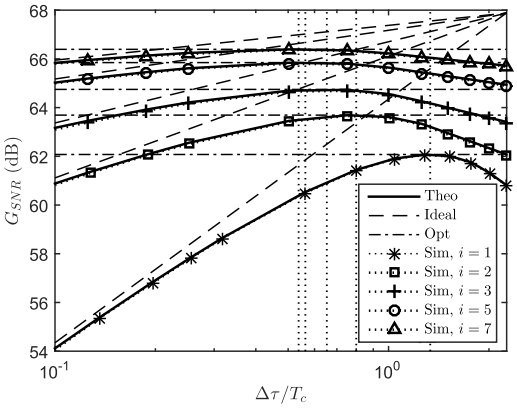

FIGURE 6. SNR gain versus CPM.

given $\Delta\tau$. In addition, the SNR gain reaches its optimal value when $\Delta\tau = a_i T_{opt}^i/i!$, $i = 1, 2, 3, 5, 7$ (which correspond to the dotted vertical lines, from right to left).

3) TIME SYNCHRONIZATION ERROR AND THRESHOLD TIME

Fig. 7 illustrates the time synchronization error as a function of CPM. The dotted vertical lines in this figure correspond (from left to right) to the threshold integration times $\Delta\tau \geq a_i T_{th}^i/i!$ $(i = 7, 5, 3, 2, 1)$, respectively. As shown, the time synchronization error initially increases with $\Delta\tau$, and then stabilizes when $\Delta\tau \geq a_i T_{th}^i/i!$ and $i > 1$, which agrees well with (19). The shadowed area is the range of ε_τ when $\Delta\tau \geq a_1 T_{th}$ and $i = 1$. In addition, when the motion order is higher than three, the largest synchronization error is less than $T_c/5$, which is in general sufficient to meet the acquisition requirements, and can therefore be neglected.

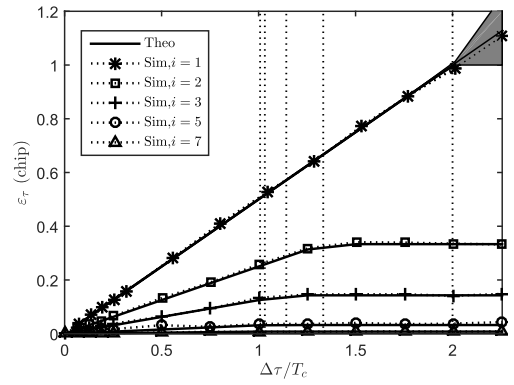

FIGURE 7. Time synchronization error versus CPM.

B. NUMERICAL EVALUATION OF THE DFM EFFECT

Numerical simulations were conducted to evaluate the integration performance in the presence of DFM, and thus verify the expressions derived above. In these simulations, the sampling rate was set to 1 MHz, and the FFT algorithm was used to achieve coherent accumulation with Doppler frequency search. To mitigate the picket fence effect, the time sequences were zero-padded to four times their original length before performing the FFT. To simulate large time-bandwidth product conditions, BT_K ranged from 10 to 10^5, with $T_K = 0.1$ s; in small time-bandwidth product conditions, the normalized motion parameter $a_i f_0$ ranged from 10^2 to 10^4, with $f_0 = 1.575$ GHz. The respective motion parameters for different motion orders (i.e., a_i) were determined.

1) LARGE TIME-BANDWIDTH PRODUCT CONDITIONS

Fig. 8 illustrates the integration loss caused by DFM in large time-bandwidth product conditions. The simulation results obtained for different motion orders are represented by dotted lines with different markers. They all coincide with the theoretical results obtained with (26), which are represented by solid lines. As shown in this figure, the integration loss increases with BT_K and decreases with the order of motion.

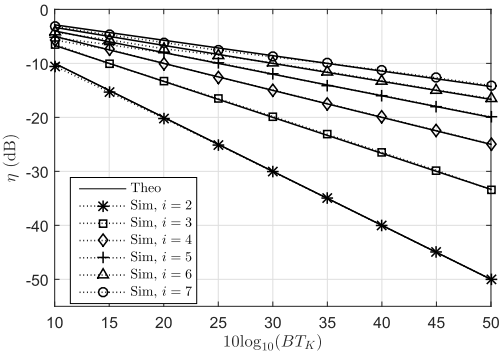

FIGURE 8. Integration loss caused by DFM in large time-bandwidth product conditions.

2) SMALL TIME-BANDWIDTH PRODUCT CONDITIONS

Simulations were also carried out to test the fitting equations presented above for the case of small time-bandwidth product conditions. The simulation results are shown in Figs. 9 to 11. In these figures the legend entry "Fit" stands for the numerical fitting case.

Fig. 9 shows the behavior of the optimal SNR gain with DFM in small time-bandwidth product conditions. As shown, the optimal SNR decreases linearly as $10\log_{10}(a_i f_0)$ increases, which agrees well with (31).

Fig. 10 shows the integration loss caused by DFM in small time-bandwidth product conditions. As shown, the integration loss increases with the time-bandwidth product and decreases with the order of motion, which agrees with (34).

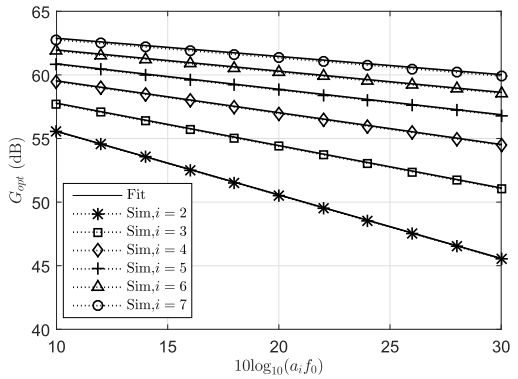

FIGURE 9. Optimal SNR gain with DFM in small time-bandwidth product conditions.

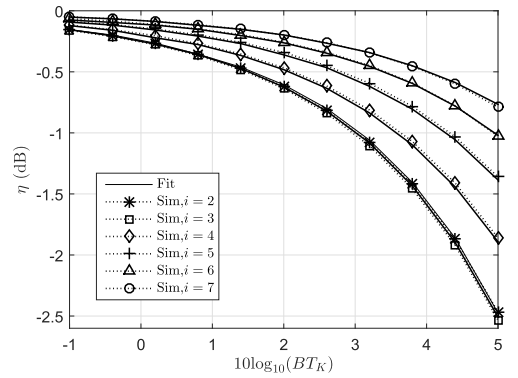

FIGURE 10. Integration loss caused by DFM in small time-bandwidth product conditions.

The frequency synchronization error caused by DFM is related to $a_i f_0$. As an illustrative example, the frequency synchronization error when $10\log_{10}(a_i f_0) = 20$ is examined in Fig. 11. As shown, the frequency synchronization error increases with the time-bandwidth product, which agrees with (35).

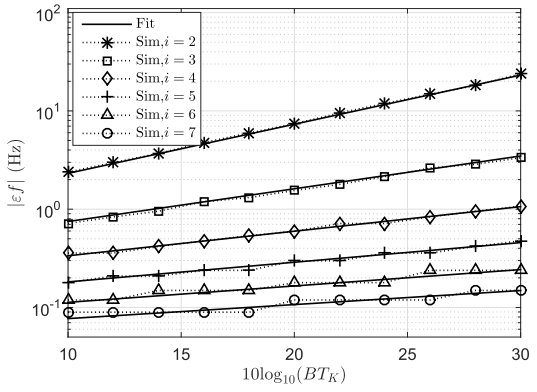

FIGURE 11. Frequency synchronization error caused by DFM when $10\log_{10}(a_i f_0) = 20$.

The derivatives of η and $\varepsilon_\tau/\varepsilon_f$ show that, for the same CPM/DFM, the higher the motion order, the smaller the integration loss and synchronization error, which agrees well with the simulation results. It can therefore be concluded that the CPM/DFM effects are mainly dictated by the lower-order motions, which validates the finite order approximation using the Weierstrass approximation principle [8]. This behavior provides theoretical guidance for integration performance analysis in the presence of CPM/DFM, for motion order configuration when modeling the received signal, and for selection and evaluation of the dynamic focus algorithm. The latter two functions are illustrated in the next subsection.

C. NUMERICAL RESULTS IN SPECIFIC CONDITIONS

To sum up the above analyses, we conducted a quantitative effect analysis for each order motion and particular integration times.

The modulated PN code and carrier frequency were set as above, and integration times of 0.1 and 1 s were used. The motion parameter values corresponding to an integration loss of 1 dB are shown in Table 1.

TABLE 1. Motion parameter values for 1 dB integration loss.

Motion order		1	2	3	4
CPM	$T_K = 0.1$ s	1.276 km/s	25.51 km/s^2	874.7 km/s^3	40820 km/s^4
	$T_K = 1$ s	127.6 m/s	255.1 m/s^2	874.7 m/s^3	4.082 km/s^4
DFM	$T_K = 0.1$ s	—	38.48 m/s^2	756.9 m/s^3	26.22 km/s^4
	$T_K = 1$ s	—	0.3848 m/s^2	0.7569 m/s^3	2.622 m/s^4

Table 1 illustrates the fact that, when the integration time is 0.1 s, only when the acceleration exceeds 25.51 km/s^2 or the jerk exceeds 756.9 m/s^3 will the effect of CPM and DFM cause a 1 dB integration loss. However, these motion values are not verified in practical situations. Therefore, the influence on integration performance of the CPM related to second-order motion and above, and of the DFM related to third-order motion and above can be neglected in this case. In other words, only the first-order CPM and second-order DFM need to be considered. Therefore, a second-order motion model can satisfy the motion modeling requirements, and the corresponding dynamic focus algorithm is sufficient.

When the integration time is 1 s, only when the acceleration exceeds 255.1 m/s^2 or the jerk exceeds 0.757 m/s^3 will the effect of CPM and DFM cause a 1 dB integration loss. In this case, the first- and second-order CPM effects, and the second- and third-order DFM effects are relevant and must be considered. Therefore, in this case, a signal model with third-order motion and a dynamic focus algorithm suitable for third-order motion models should be used.

As seen from the above discussion, the performance analysis proposed in this paper provides theoretical guidance for motion order configuration when modeling specific received signals, as well as for selection and evaluation of the dynamic focus algorithm.

VI. CONCLUSION

This paper presented closed-form analytic expressions for the integration of DSSS signals with CPM, and numerically fitted equations for the integration performance in the presence of DFM. The CPM and DFM effects were analyzed in

terms of integration loss, synchronization error, SNR gain, and optimal integration time. The main contribution of this paper was the extension to higher-order motion situations of the integration performance analyses previously existing for the specific cases of second- and third-order motion, and the derivation of generalized equations applicable to motions of arbitrary order. All derivations were verified by simulation. This study provides guidance for motion order selection when modeling the received DSSS signals and, in general, to the receiver design process. It can also be used to evaluate both the performance of integration methods in the presence of CPM/DFM and that of CPM/DFM mitigation methods. The effect of pulse shaping will be addressed in a further study.

APPENDIX A
PROOF OF (11)

The summation is a discrete expression of the integral. Therefore, for analytical simplification, it is replaced by an integral operation in the following derivations. We will take Case 1 ($0 \le \Delta\tau \le T_c$) as an example herein. The integral is a piecewise function of $\delta\tau$, which can be divided into six sections according to the intersection points marked by the dots in Fig. 3.

A. SECTION 1: $-T_c \le \delta\tau < \Delta\tau - T_c$

When $-T_c \le \delta\tau < \Delta\tau - T_c$, the cross section is located in the region labeled ① in Fig. 3(a), and the upper integration limit (denoted by T_{k_u}) can be obtained by

$$\delta\tau - \frac{a_i}{i!}\left(T_{k\_u}\right)^i = -T_c. \tag{A.1}$$

Therefore, we obtain the upper limit $T_{k\_u}=[(T_c+\delta\tau)\, i!/a_i]^{1/i} = \left[(T_c+\delta\tau)/\Delta\tau\right]^{1/i} T_K$, and the integral becomes

$$\begin{aligned} S(\delta\tau) &= \frac{1}{T_K}\int_0^{T_K} R_c\left[\delta\tau - \frac{a_i}{i!}(T_k)^i\right]dT_k \\ &= \frac{1}{T_K}\int_0^{T_{k\_u}} \left\{1 + \left[\delta\tau - \frac{a_i}{i!}(T_k)^i\right]\Big/T_c\right\}dT_k \\ &= \frac{i\,(T_c+\delta\tau)^{\frac{i+1}{i}}}{(i+1)\,T_c\,(\Delta\tau)^{\frac{1}{i}}}. \end{aligned} \tag{A.2}$$

The relationship $\Delta\tau = a_i (T_K)^i/i!$ has been used in the derivation.

B. SECTION 2: $\Delta\tau - T_c \le \delta\tau < 0$

When $\Delta\tau - T_c \le \delta\tau < 0$, the cross section is located in the region labeled ② in Fig. 3(b), and the integral becomes

$$\begin{aligned} S(\delta\tau) &= \frac{1}{T_K}\int_0^{T_K} R_c\left[\delta\tau - \frac{a_i}{i!}(T_k)^i\right]dT_k \\ &= \frac{1}{T_K}\int_0^{T_K} \left\{1 + \left[\delta\tau - \frac{a_i}{i!}(T_k)^i\right]\Big/T_c\right\}dT_k \\ &= 1 + [(i+1)\,\delta\tau - \Delta\tau]/[(i+1)\,T_c]. \end{aligned} \tag{A.3}$$

C. SECTION 3: $0 \le \delta\tau < \Delta\tau$

When $0 \le \delta\tau < \Delta\tau$, the cross section is located in the region labeled ③ in Fig. 3(c), and the integration limit corresponding to the peak of the correlation function (denoted by T_{k_p}) can be obtained by

$$\delta\tau - \frac{a_i}{i!}\left(T_{k\_p}\right)^i = 0. \tag{A.4}$$

Therefore, we obtain $T_{k\_p} = \left(i!\delta\tau/a_i\right)^{1/i} = \left(\delta\tau/\Delta\tau\right)^{1/i} T_K$, and the integral becomes

$$\begin{aligned} S(\delta\tau) &= \frac{1}{T_K}\int_0^{T_K} R_c\left[\delta\tau - \frac{a_i}{i!}(T_k)^i\right]dT_k \\ &= \frac{1}{T_K}\int_0^{T_{k\_p}} \left\{1 - \left[\delta\tau - \frac{a_i}{i!}(T_k)^i\right]\Big/T_c\right\}dT_k \\ &\quad + \frac{1}{T_K}\int_{T_{k\_p}}^{T_K} \left\{1 + \left[\delta\tau - \frac{a_i}{i!}(T_k)^i\right]\Big/T_c\right\}dT_k \\ &= 1 - \frac{2i\,(\delta\tau)^{\frac{i+1}{i}} + (\Delta\tau)^{\frac{i+1}{i}} - (i+1)\,\delta\tau\,(\Delta\tau)^{\frac{1}{i}}}{(i+1)\,T_c\,(\Delta\tau)^{\frac{1}{i}}}. \end{aligned} \tag{A.5}$$

D. SECTION 4: $\Delta\tau \le \delta\tau < T_c$

When $\Delta\tau \le \delta\tau < T_c$, the cross section is located in the region labeled ④ in Fig. 3(d), and the integral becomes

$$\begin{aligned} S(\delta\tau) &= \frac{1}{T_K}\int_0^{T_K} R_c\left[\delta\tau - \frac{a_i}{i!}(T_k)^i\right]dT_k \\ &= \frac{1}{T_K}\int_0^{T_K} \left\{1 - \left[\delta\tau - \frac{a_i}{i!}(T_k)^i\right]\Big/T_c\right\}dT_k \\ &= 1 + [\Delta\tau - (i+1)\,\delta\tau]/[(i+1)\,T_c]. \end{aligned} \tag{A.6}$$

E. SECTION 5: $T_c \le \delta\tau \le \Delta\tau + T_c$

When $T_c \le \delta\tau \le \Delta\tau + T_c$, the cross section is located in the region labeled ⑤ in Fig. 3(e), and the lower integration limit (denoted by T_{k_l}) can be obtained by

$$\delta\tau - \frac{a_i}{i!}\left(T_{k\_l}\right)^i = T_c. \tag{A.7}$$

Therefore, we obtain the lower limit $T_{k\_l} = \left[(\delta\tau - T_c)\, i!/a_i\right]^{1/i} = \left[(\delta\tau - T_c)/\Delta\tau\right]^{1/i} T_K$, and the integral becomes

$$\begin{aligned} S(\delta\tau) &= \frac{1}{T_K}\int_0^{T_K} R_c\left[\delta\tau - \frac{a_i}{i!}(T_k)^i\right]dT_k \\ &= \frac{1}{T_K}\int_{T_{k\_l}}^{T_K} \left\{1 - \left[\delta\tau - \frac{a_i}{i!}(T_k)^i\right]\Big/T_c\right\}dT_k \\ &= 1 + \frac{i\,(\delta\tau - T_c)^{\frac{i+1}{i}} + (\Delta\tau)^{\frac{i+1}{i}} - (i+1)\,\delta\tau\,(\Delta\tau)^{\frac{1}{i}}}{(i+1)\,T_c\,(\Delta\tau)^{\frac{1}{i}}} \end{aligned} \tag{A.8}$$

F. SECTION 6: $\delta\tau > \Delta\tau + T_c$ or $\delta\tau < -T_c$

Finally, when $\delta\tau > \Delta\tau + T_c$ or $\delta\tau < -T_c$, the cross section is located in the region labeled ⑥, and the integral

becomes

$$S(\delta\tau) = \frac{1}{T_K}\int_0^{T_K} R_c\left[\delta\tau - \frac{a_i}{i!}(T_k)^i\right]dT_k = 0. \tag{A.9}$$

Summarizing, the results of the integration are

$$S(\delta\tau) = \begin{cases} \dfrac{i(T_c+\delta\tau)^{\frac{i+1}{i}}}{(i+1)T_c(\Delta\tau)^{\frac{1}{i}}}, & -T_c \le \delta\tau < \Delta\tau - T_c \\ 1 - \dfrac{\Delta\tau - (i+1)\delta\tau}{(i+1)T_c}, & \Delta\tau - T_c \le \delta\tau < 0 \\ 1 - \dfrac{2i(\delta\tau)^{\frac{i+1}{i}} + (\Delta\tau)^{\frac{i+1}{i}} - (i+1)\delta\tau(\Delta\tau)^{\frac{1}{i}}}{(i+1)T_c(\Delta\tau)^{\frac{1}{i}}}, & 0 \le \delta\tau < \Delta\tau \\ 1 + \dfrac{\Delta\tau - (i+1)\delta\tau}{(i+1)T_c}, & \Delta\tau \le \delta\tau < T_c \\ 1 + \dfrac{i(\delta\tau - T_c)^{\frac{i+1}{i}} + (\Delta\tau)^{\frac{i+1}{i}} - (i+1)\delta\tau(\Delta\tau)^{\frac{1}{i}}}{(i+1)T_c(\Delta\tau)^{\frac{1}{i}}}, & T_c \le \delta\tau \le \Delta\tau + T_c \\ 0, & \text{others.} \end{cases} \tag{A.10}$$

APPENDIX B
PROOF OF (14)–(19)

To obtain the maximum $S(\delta\tau)$ presented in (25), we first examine the derivatives of $S(\delta\tau)$.

Case 1 ($0 \le \Delta\tau < T_c$):

When $0 \le \Delta\tau < T_c$, the derivative of the integration result with respect to $\delta\tau$ is given by

$$\frac{\partial S(\delta\tau)}{\partial \delta\tau} = \begin{cases} \dfrac{(T_c+\delta\tau)^{\frac{1}{i}}}{T_c(\Delta\tau)^{\frac{1}{i}}} > 0, & -T_c \le \delta\tau < \Delta\tau - T_c \\ \dfrac{1}{T_c} > 0, & \Delta\tau - T_c \le \delta\tau < 0 \\ \dfrac{-2(\delta\tau)^{\frac{1}{i}} + (\Delta\tau)^{\frac{1}{i}}}{T_c(\Delta\tau)^{\frac{1}{i}}}, & 0 \le \delta\tau < \Delta\tau \\ -\dfrac{1}{T_c} < 0, & \Delta\tau \le \delta\tau < T_c \\ \dfrac{-(\Delta\tau)^{\frac{1}{i}} + (\delta\tau - T_c)^{\frac{1}{i}}}{T_c(\Delta\tau)^{\frac{1}{i}}} \le \dfrac{(\Delta\tau)^{\frac{1}{i}} - (\Delta\tau)^{\frac{1}{i}}}{T_c(\Delta\tau)^{\frac{1}{i}}} = 0, & T_c \le \delta\tau \le \Delta\tau + T_c \\ 0, & \text{others.} \end{cases} \tag{B.1}$$

Therefore, $S(\delta\tau)$ first increases with $\delta\tau$ when $\delta\tau < 0$, and then decreases with $\delta\tau$ when $\delta\tau \ge \Delta\tau$. Furthermore, when $0 \le \delta\tau < \Delta\tau$, the derivative of $S(\delta\tau)$ is a monotonically decreasing function of $\delta\tau$ and crosses zero. Therefore, the maximum of $S(\delta\tau)$ is located at the zero crossing point within the region $0 \le \delta\tau < \Delta\tau$. Setting the derivatives of $S(\delta\tau)$ in this region to zero, we can obtain the zero crossing point as follows:

$$\begin{cases} \dfrac{-2(\delta\tau)^{\frac{1}{i}} + (\Delta\tau)^{\frac{1}{i}}}{T_c(\Delta\tau)^{\frac{1}{i}}} = 0 \\ 0 \le \delta\tau < \Delta\tau \end{cases} \Rightarrow \delta\tau = \frac{\Delta\tau}{2^i}. \tag{B.2}$$

The maximum value of $S(\delta\tau)$ in this case therefore becomes

$$S\left(\frac{\Delta\tau}{2^i}\right) = 1 - \frac{1-2^{-i}}{i+1}\frac{\Delta\tau}{T_c} \tag{B.3}$$

The integration loss and synchronization error can therefore be found to be

$$\eta = \max_{\delta\tau}\left\{|S(\delta\tau)|^2\right\} = \left(1 - \frac{1-2^{-i}}{i+1}\frac{\Delta\tau}{T_c}\right)^2 \tag{B.4}$$

and

$$\varepsilon_\tau = \arg\max_{\delta\tau}\left\{|S(\delta\tau)|^2\right\} = \frac{\Delta\tau}{2^i}. \tag{B.5}$$

Case 2 ($T_c \le \Delta\tau < 2T_c$):

When $T_c \le \Delta\tau < 2T_c$, the derivative of the integration result with respect to $\delta\tau$ is given by

$$\frac{\partial S(\delta\tau)}{\partial \delta\tau} = \begin{cases} \dfrac{(T_c+\delta\tau)^{\frac{1}{i}}}{T_c(\Delta\tau)^{\frac{1}{i}}} \ge 0, & -T_c \le \delta\tau < 0 \\ \dfrac{(T_c+\delta\tau)^{\frac{1}{i}} - 2(\delta\tau)^{\frac{1}{i}}}{T_c(\Delta\tau)^{\frac{1}{i}}}, & 0 \le \delta\tau < \Delta\tau - T_c \\ \dfrac{-2(\delta\tau)^{\frac{1}{i}} + (\Delta\tau)^{\frac{1}{i}}}{T_c(\Delta\tau)^{\frac{1}{i}}}, & \Delta\tau - T_c \le \delta\tau < T_c \\ \dfrac{-2(\delta\tau)^{\frac{1}{i}} + (\Delta\tau)^{\frac{1}{i}} + (\delta\tau - T_c)^{\frac{1}{i}}}{T_c(\Delta\tau)^{\frac{1}{i}}}, & T_c \le \delta\tau < \Delta\tau \\ \dfrac{-(\Delta\tau)^{\frac{1}{i}} + (\delta\tau - T_c)^{\frac{1}{i}}}{T_c(\Delta\tau)^{\frac{1}{i}}} \le \dfrac{-(\Delta\tau)^{\frac{1}{i}} + (\Delta\tau)^{\frac{1}{i}}}{T_c(\Delta\tau)^{\frac{1}{i}}} = 0, & \Delta\tau \le \delta\tau \le \Delta\tau + T_c \\ 0, & \text{others.} \end{cases} \tag{B.6}$$

In this case, three distinct sections shall be discussed in detail.

A. SECTION 4: $T_c \le \delta\tau < \Delta\tau$

When $T_c \le \delta\tau < \Delta\tau$, we can obtain $\Delta\tau < 2T_c \le T_c + \delta\tau$. In addition, because $T_c/\delta\tau \le 1$, using a Taylor expansion for $i > 1$ we obtain

$$(T_c+\delta\tau)^{\frac{1}{i}} + (\delta\tau - T_c)^{\frac{1}{i}} = (\delta\tau)^{\frac{1}{i}}\left[\left(1+\frac{T_c}{\delta\tau}\right)^{\frac{1}{i}} + \left(1-\frac{T_c}{\delta\tau}\right)^{\frac{1}{i}}\right]$$

$$
\begin{aligned}
&= (\delta\tau)^{\frac{1}{i}}\left[1+\frac{1}{i}\left(\frac{T_c}{\delta\tau}\right)+\frac{1}{2!}\frac{1}{i}\left(\frac{1}{i}-1\right)\left(\frac{T_c}{\delta\tau}\right)^2\right.\\
&\quad+\frac{1}{3!}\frac{1}{i}\left(\frac{1}{i}-1\right)\left(\frac{1}{i}-2\right)\left(\frac{T_c}{\delta\tau}\right)^3\\
&\quad+\frac{1}{4!}\frac{1}{i}\left(\frac{1}{i}-1\right)\left(\frac{1}{i}-2\right)\left(\frac{1}{i}-3\right)\left(\frac{T_c}{\delta\tau}\right)^4+\cdots\\
&\quad+1-\frac{1}{i}\left(\frac{T_c}{\delta\tau}\right)+\frac{1}{2!}\frac{1}{i}\left(\frac{1}{i}-1\right)\left(\frac{T_c}{\delta\tau}\right)^2\\
&\quad-\frac{1}{3!}\frac{1}{i}\left(\frac{1}{i}-1\right)\left(\frac{1}{i}-2\right)\left(\frac{T_c}{\delta\tau}\right)^3\\
&\quad\left.+\frac{1}{4!}\frac{1}{i}\left(\frac{1}{i}-1\right)\left(\frac{1}{i}-2\right)\left(\frac{1}{i}-3\right)\left(\frac{T_c}{\delta\tau}\right)^4+..\right]\\
&= (\delta\tau)^{\frac{1}{i}}\left\{2+2\left[\frac{1}{2!}\frac{1}{i}\left(\frac{1}{i}-1\right)\left(\frac{T_c}{\delta\tau}\right)^2\right.\right.\\
&\quad\left.\left.+\frac{1}{4!}\frac{1}{i}\left(\frac{1}{i}-1\right)\left(\frac{1}{i}-2\right)\left(\frac{1}{i}-3\right)\left(\frac{T_c}{\delta\tau}\right)^4+\cdots\right]\right\}\\
&< 2(\delta\tau)^{\frac{1}{i}}. \qquad \text{(B.7)}
\end{aligned}
$$

If $i=1$, we can obtain $-2(\delta\tau)^{\frac{1}{i}}+(\Delta\tau)^{\frac{1}{i}}+(\delta\tau-T_c)^{\frac{1}{i}}=-\delta\tau+\Delta\tau-T_c<0$. Therefore, as stated in (B.6), $\frac{\partial S(\delta\tau)}{\partial\delta\tau}\Big|_{T_c\le\delta\tau<\Delta\tau}\le\frac{-2(\delta\tau)^{\frac{1}{i}}+(T_c+\delta\tau)^{\frac{1}{i}}+(\delta\tau-T_c)^{\frac{1}{i}}}{T_c(\Delta\tau)^{\frac{1}{i}}}<0$.

B. SECTION 3: $\Delta\tau - T_c \le \delta\tau < T_c$

When $\Delta\tau - T_c \le \delta\tau < T_c$, the sign of the derivative is given by

$$
\begin{aligned}
\operatorname{sign}\left\{\frac{-2(\delta\tau)^{\frac{1}{i}}+(\Delta\tau)^{\frac{1}{i}}}{T_c(\Delta\tau)^{\frac{1}{i}}}\right\} &= \operatorname{sign}\left\{-2(\delta\tau)^{\frac{1}{i}}+(\Delta\tau)^{\frac{1}{i}}\right\}\\
&= \operatorname{sign}\left\{-2^i(\delta\tau)+\Delta\tau\right\}, \qquad \text{(B.8)}
\end{aligned}
$$

where $\operatorname{sign}\{x\}$ denotes the sign of x. Since $\Delta\tau - T_c \le \delta\tau < T_c$, we have $-2^i(\delta\tau)+\Delta\tau \le -2^i(\Delta\tau - T_c)+\Delta\tau = 2^iT_c-\left(2^i-1\right)\Delta\tau$. If $\Delta\tau \ge T_c/\left(1-2^{-i}\right)$, the derivative is always negative within this region. Therefore, the maximum value is $S(\Delta\tau - T_c)$. If $\Delta\tau < T_c/\left(1-2^{-i}\right)$, the derivative is a monotonically decreasing function of $\delta\tau$ and crosses zero; the maximum value of $S(\delta\tau)$ will then be given by

$$
S\left(\frac{\Delta\tau}{2^i}\right) = 1-\frac{1-2^{-i}}{i+1}\frac{\Delta\tau}{T_c}. \qquad \text{(B.9)}
$$

C. SECTION 2: $0 \le \delta\tau < \Delta\tau - T_c$

When $0 \le \delta\tau < \Delta\tau - T_c$, the sign of the derivative is given by

$$
\begin{aligned}
&\operatorname{sign}\left\{\frac{(T_c+\delta\tau)^{\frac{1}{i}}-2(\delta\tau)^{\frac{1}{i}}}{T_c(\Delta\tau)^{\frac{1}{i}}}\right\}\\
&\quad= \operatorname{sign}\left\{(T_c+\delta\tau)^{\frac{1}{i}}-2(\delta\tau)^{\frac{1}{i}}\right\}\\
&\quad= \operatorname{sign}\left\{(T_c+\delta\tau)-2^i\delta\tau\right\}\\
&\quad= \operatorname{sign}\left\{T_c-\left(2^i-1\right)\delta\tau\right\}. \qquad \text{(B.10)}
\end{aligned}
$$

Given that $0 \le \delta\tau < \Delta\tau - T_c$, we have that $T_c-\left(2^i-1\right)\delta\tau > T_c-\left(2^i-1\right)(\Delta\tau - T_c) = 2^iT_c-\left(2^i-1\right)\Delta\tau$.

If $\Delta\tau < T_c/\left(1-2^{-i}\right)$, the derivative is always positive within this region. Therefore, the maximum value is $S(\Delta\tau - T_c)$. If $\Delta\tau \ge T_c/\left(1-2^{-i}\right)$ and $0 \le \delta\tau < T_c/\left(2^i-1\right)$, the derivative is positive; therefore, if $\Delta\tau \ge T_c/\left(1-2^{-i}\right)$ and the derivative is non-positive, $0 \le \delta\tau < \Delta\tau - T_c$ and the maximum value of $S(\delta\tau)$ is

$$
S\left(\frac{T_c}{2^i-1}\right) = \frac{i}{i+1}\left[\frac{T_c}{\left(1-2^{-i}\right)\Delta\tau}\right]^{\frac{1}{i}}. \qquad \text{(B.11)}
$$

Consequently, the maximum value of $S(\delta\tau)$ is a piecewise function of $\Delta\tau$ that can be expressed as

$$
\begin{aligned}
&\max\{S(\delta\tau)\}\\
&= \begin{cases} S\left(\frac{\Delta\tau}{2^i}\right) = 1-\frac{1-2^{-i}}{i+1}\frac{\Delta\tau}{T_c}, & T_c \le \Delta\tau < \frac{T_c}{1-2^{-i}}\\ S\left(\frac{T_c}{2^i-1}\right) = \frac{i}{i+1}\left[\frac{T_c}{\left(1-2^{-i}\right)\Delta\tau}\right]^{\frac{1}{i}}, & \frac{T_c}{1-2^{-i}} \le \Delta\tau < 2T_c. \end{cases}
\end{aligned} \qquad \text{(B.12)}
$$

The integration loss and synchronization error can then be found to be

$$
\begin{aligned}
\eta &= \max_{\delta\tau}\left\{|S(\delta\tau)|^2\right\}\\
&= \begin{cases} \left(1-\frac{1-2^{-i}}{i+1}\frac{\Delta\tau}{T_c}\right)^2, & T_c \le \Delta\tau < \frac{T_c}{1-2^{-i}}\\ \left\{\frac{i}{i+1}\left[\frac{T_c}{\left(1-2^{-i}\right)\Delta\tau}\right]^{\frac{1}{i}}\right\}^2, & \frac{T_c}{1-2^{-i}} \le \Delta\tau < 2T_c \end{cases}
\end{aligned} \qquad \text{(B.13)}
$$

and

$$
\begin{aligned}
\varepsilon_\tau &= \arg\max_{\delta\tau}\left\{|S(\delta\tau)|^2\right\}\\
&= \begin{cases} \frac{\Delta\tau}{2^i}, & T_c \le \Delta\tau < \frac{T_c}{1-2^{-i}}\\ \frac{T_c}{2^i-1}, & \frac{T_c}{1-2^{-i}} \le \Delta\tau < 2T_c. \end{cases}
\end{aligned} \qquad \text{(B.14)}
$$

Case 3 ($\Delta\tau \ge 2T_c$):

When $\Delta\tau \ge 2T_c$, the derivative of the integration result with respect to $\delta\tau$ is given by

$$
\frac{\partial S(\delta\tau)}{\partial\delta\tau}
$$

$$= \begin{cases} \dfrac{(T_c+\delta\tau)^{\frac{1}{i}}}{T_c(\Delta\tau)^{\frac{1}{i}}} \geq 0, & -T_c \leq \delta\tau < 0 \\ \dfrac{(T_c+\delta\tau)^{\frac{1}{i}} - 2(\delta\tau)^{\frac{1}{i}}}{T_c(\Delta\tau)^{\frac{1}{i}}}, & 0 \leq \delta\tau < T_c \\ \dfrac{(T_c+\delta\tau)^{\frac{1}{i}} + (\delta\tau - T_c)^{\frac{1}{i}} - 2(\delta\tau)^{\frac{1}{i}}}{T_c(\Delta\tau)^{\frac{1}{i}}}, & T_c \leq \delta\tau < \Delta\tau - T_c \\ \dfrac{-2(\delta\tau)^{\frac{1}{i}} + (\Delta\tau)^{\frac{1}{i}} + (\delta\tau - T_c)^{\frac{1}{i}}}{T_c(\Delta\tau)^{\frac{1}{i}}} & \\ \leq \dfrac{-2(\delta\tau)^{\frac{1}{i}} + (T_c+\delta\tau)^{\frac{1}{i}} + (\delta\tau - T_c)^{\frac{1}{i}}}{T_c(\Delta\tau)^{\frac{1}{i}}} \leq 0, & \Delta\tau - T_c \leq \delta\tau < \Delta\tau \\ \dfrac{-(\Delta\tau)^{\frac{1}{i}} + (\delta\tau - T_c)^{\frac{1}{i}}}{T_c(\Delta\tau)^{\frac{1}{i}}} \leq \dfrac{-(\Delta\tau)^{\frac{1}{i}} + (\Delta\tau_c)^{\frac{1}{i}}}{T_c(\Delta\tau)^{\frac{1}{i}}} = 0, & \Delta\tau \leq \delta\tau \leq \Delta\tau + T_c \\ 0, & \text{others.} \end{cases} \tag{B.15}$$

In this case, two distinct sections shall be discussed in detail.

D. SECTION 2: $0 \leq \delta\tau < T_c$

As stated in Case 2, Section 2, when $\Delta\tau \geq 2T_c$ the derivative is first positive (when $0 \leq \delta\tau < T_c/(2^i-1)$), and then non-positive (when $T_c/(2^i-1) \leq \delta\tau < \Delta\tau - T_c$). Therefore, the maximum value of $S(\delta\tau)$ is

$$S\left(\frac{T_c}{2^i-1}\right) = \frac{i}{i+1}\left[\frac{T_c}{\left(1-2^{-i}\right)\Delta\tau}\right]^{\frac{1}{i}}. \tag{B.16}$$

E. SECTION 3: $T_c \leq \delta\tau < \Delta\tau - T_c$

As stated in Case 2, Section 4, when $i > 1$ a Taylor expansion shows that the derivative is always negative. If $i = 1$, we have that $-2(\delta\tau)^{\frac{1}{i}} + (\delta\tau + T_c)^{\frac{1}{i}} + (\delta\tau - T_c)^{\frac{1}{i}} = 0$, and the derivative is therefore zero. Consequently, the maximum value of $S(\delta\tau)$ is

$$\max\{S(\delta\tau)\} = \frac{i}{i+1}\left[\frac{T_c}{\left(1-2^{-i}\right)\Delta\tau}\right]^{\frac{1}{i}}. \tag{B.17}$$

The integration loss and synchronization error can therefore be found to be

$$\eta = \max_{\delta\tau}\left\{|S(\delta\tau)|^2\right\} = \left\{\frac{i}{i+1}\left[\frac{T_c}{\left(1-2^{-i}\right)\Delta\tau}\right]^{\frac{1}{i}}\right\}^2 \tag{B.18}$$

and

$$\varepsilon_\tau = \arg\max_{\delta\tau}\left\{|S(\delta\tau)|^2\right\} = \begin{cases} \dfrac{T_c}{2^i-1}, & i > 1 \\ [T_c, \Delta\tau - T_c], & i = 1. \end{cases} \tag{B.19}$$

Combining (B.4), (B.13), and (B.18), the integration loss can be obtained as

$$\eta = \max_{\delta\tau}\left\{|S(\delta\tau)|^2\right\} = \begin{cases} \left(1 - \dfrac{1-2^{-i}}{i+1}\dfrac{\Delta\tau}{T_c}\right)^2, & 0 \leq \Delta\tau < \dfrac{T_c}{1-2^{-i}} \\ \left(\dfrac{i}{i+1}\left[\dfrac{T_c}{\left(1-2^{-i}\right)\Delta\tau}\right]^{1/i}\right)^2, & \Delta\tau \geq \dfrac{T_c}{1-2^{-i}}. \end{cases} \tag{B.20}$$

Similarly, the synchronization error can be obtained by combining (B.5), (B.14), and (B.19), resulting in

$$\varepsilon_\tau = \arg\max_{\delta\tau}\left\{|S(\delta\tau)|^2\right\} = \begin{cases} \dfrac{\Delta\tau}{2^i}, & 0 \leq \Delta\tau < \dfrac{T_c}{1-2^{-i}} \\ \dfrac{T_c}{2^i-1}, & \Delta\tau \geq \dfrac{T_c}{1-2^{-i}} \text{ and } i > 1 \\ [T_c, \Delta\tau - T_c], & \Delta\tau \geq 2T_c \text{ and } i = 1. \end{cases} \tag{B.21}$$

REFERENCES

[1] T. Ren and M. G. Petovello, "A stand-alone approach for high-sensitivity GNSS receivers in signal-Challenged environment," *IEEE Trans. Aerosp. Electron. Syst.*, vol. 53, no. 5, pp. 2438–2448, Oct. 2017.

[2] P. Huang, G. Liao, Z. Yang, X.-G. Xia, J.-T. Ma, and J. Ma, "Long-time coherent integration for weak maneuvering target detection and high-order motion parameter estimation based on keystone transform," *IEEE Trans. Signal Process.*, vol. 64, no. 15, pp. 4013–4026, Aug. 2016.

[3] X. Li, G. Cui, W. Yi, and L. Kong, "A fast maneuvering target motion parameters estimation algorithm based on ACCF," *IEEE Signal Process. Lett.*, vol. 22, no. 3, pp. 270–274, Mar. 2015.

[4] J. Xu, J. Yu, Y.-N. Peng, and X. Xia, "Radon-Fourier transform for radar target detection, I: Generalized Doppler filter bank," *IEEE Trans. Aerosp. Elecron. Syst.*, vol. 47, no. 2, pp. 1186–1202, Apr. 2011.

[5] N. Petrov, F. L. Chevalier, and A. G. Yarovoy, "Detection of range migrating targets in compound-Gaussian clutter," *IEEE Trans. Aerosp. Electron. Syst.*, vol. 54, no. 1, pp. 37–50, Feb. 2018.

[6] J. Zheng, J. Zhang, S. Xu, H. Liu, and Q. H. Liu, "Radar detection and motion parameters estimation of maneuvering target based on the extended keystone transform," *IEEE Access*, vol. 6, pp. 76060–76074, Nov. 2018. doi: 10.1109/ACCESS.2018.2881204.

[7] R. Tian, C. Lin, Q. Bao, and Z. Chen, "Coherent integration method of high-speed target for frequency agile radar," *IEEE Access*, vol. 6, pp. 18984–18993, 2018.

[8] X. Chen, J. Guan, N. Liu, and Y. He, "Maneuvering target detection via radon-fractional Fourier transform-based long-time coherent integration," *IEEE Trans. Signal Process.*, vol. 62, no. 4, pp. 939–953, Feb. 2014.

[9] R. Tao, N. Zhang, and Y. Wang, "Analysing and compensating the effects of range and Doppler frequency migrations in linear frequency modulation pulse compression radar," *IET Radar, Sonar Navigat.*, vol. 5, no. 1, pp. 12–22, Jan. 2011.

[10] H. Luo, Y. Wang, Y. Luo, and S. Wu, "Analysis and compensation for the effect of code Doppler frequency in PMF-FFT algorithm," *Trans. Beijing Inst. Technol.*, vol. 33, no. 11, pp. 1176–1182, Nov. 2013.

[11] I. Djurović, V. Popović-Bugarin, and M. Simeunović, "The STFT-based estimator of micro-Doppler parameters," *IEEE Trans. Aerosp. Electron. Syst.*, vol. 53, no. 3, pp. 1273–1283, Jun. 2017.

[12] D. Li, M. Zhan, X. Zhang, Z. Fang, and H. Liu, "ISAR imaging of nonuniformly rotating target based on the multicomponent CPS model under low SNR environment," *IEEE Trans. Aerosp. Electron. Syst.*, vol. 53, no. 3, pp. 1119–1135, Jun. 2017.

[13] I. Djurović, M. Simeunović, and P. Wang, "Cubic phase function: A simple solution to polynomial phase signal analysis," *Signal Process.*, vol. 135, pp. 48–66, Jun. 2017.

[14] R. Cao, M. Li, L. Zuo, Z. Wang, and Y. Lu, "A new method for parameter estimation of high-order polynomial-phase signals," *Signal Process.*, vol. 142, pp. 212–222, Jan. 2018.
[15] Z. Zhang, H. Liu, and H. Zhang, "Joint-detection for Doppler-shift acquisition in space communications," *IEEE Commun. Lett.*, vol. 19, no. 2, pp. 215–218, Feb. 2015.
[16] J. B. Zheng, "Fast parameter estimation algorithm for cubic phase signal based on quantifying effects of Doppler frequency shift," *Prog. Electromagn. Res.*, vol. 142, no. 3, pp. 57–74, 2013.
[17] K. Sun and L. Lo Presti, "Bit sign transition cancellation method for GNSS signal acquisition," *J. Navigat.*, vol. 65, no. 1, pp. 73–97, Jan. 2012.
[18] D. Borio, "Oversampled M-sequences for joint data and bit epoch estimation in DSSS transmissions," *IEEE Commun. Lett.*, vol. 13, no. 10, pp. 721–723, Oct. 2009.
[19] G. Carluccio, F. Puggelli, and M. Albani, "Algorithm for the computation of the generalized fresnel integral," *IEEE Trans. Antennas Propag.*, vol. 59, no. 10, pp. 3943–3947, Oct. 2011.
[20] J. Xu, Y. Zuo, B. Xia, X.-G. Xia, Y.-N. Peng, and Y.-L. Wang, "Ground moving target signal analysis in complex image domain for multichannel SAR," *IEEE Trans. Geosci. Remote Sens.*, vol. 50, no. 2, pp. 538–552, Feb. 2012.
[21] A. Yasotharan and T. Thayaparan, "Strengths and limitations of the Fourier method for detecting accelerating targets by pulse Doppler radar," *IEE Proc. Radar, Sonar Navigat.*, vol. 149, no. 2, pp. 83–88, Apr. 2002.

YUYAO SHEN received the bachelor's and Ph.D. degrees from the School of Information and Electronics, Beijing Institute of Technology, Beijing, China, in 2011 and 2017, respectively. She currently holds a postdoctoral position at the Academy of Opto-Electronics, Chinese Academy of Sciences. Her research interests include spaceflight TT&C and space communication, especially spread spectrum signal processing.

YING XU received the Ph.D. degree in signal processing from the Beijing Institute of Technology, China, in 2009. She is currently a Research Professor, a Doctoral Supervisor, and the Vice Director of the Navigation Technology Research Laboratory, Academy of Opto-Electronics, Chinese Academy of Sciences. Her research interests include satellite navigation technology and its augmentation technology, and multi-source fusion localization theory and methods.